

# 1 Cassini plasma spectrometer measurements of Jovian bow shock 2 structure

3 Karoly Szego,<sup>1</sup> David T. Young,<sup>2</sup> Bruce Barraclough,<sup>3</sup> Jean-Jacques Berthelier,<sup>4</sup> Andrew  
4 J. Coates,<sup>5</sup> David J. McComas,<sup>2</sup> Frank J. Crary,<sup>2</sup> Michele K. Dougherty,<sup>6</sup> Geza Erdos,<sup>1</sup>  
5 Donald A. Gurnett,<sup>7</sup> William S. Kurth,<sup>7</sup> and Michelle F. Thomsen<sup>3</sup>

6 Received 3 June 2002; revised 18 March 2003; accepted 22 April 2003; published XX Month 2003.

7 [1] The Cassini spacecraft on its way to Saturn flew by Jupiter and crossed its bow shock  
8 more than forty times on the dusk-side of the planet, whereas the early missions targeting  
9 Jupiter explored the dawnside. Here we report the first results concerning these bow shock  
10 crossings, based on the measurements of the Cassini Plasma Spectrometer (CAPS), the  
11 magnetometer, and the radio and plasma wave science (RPWS) instrument. We present  
12 data for five bow shock crossings, one at about 1920 local time (LT), the other four  
13 between 2100 and 2130 LT,  $47.5^\circ$ – $50^\circ$  beyond terminator. During the flyby the solar  
14 activity was high and variable. The measurements confirm that the Jovian bow shock is  
15 huge, extending over  $700 R_J$  down the flank; Cassini was the first to observe such distant  
16 shock features. The bow shock was turbulent and very dynamic and magnetic fluctuations  
17 were superimposed on the shock; the downstream ion distributions exhibited bimodal  
18 structure time to time. For all bow shock crossings the onset of ion thermalization was a  
19 clear shock signature supported by an electrostatic wave signal; thermalization can be used  
20 as a signature of the shock location even in those cases when the field data are rather  
21 smeared. The strength of the shock potential weakened toward more distant regions even  
22 if the local Mach number did not decrease. Reflected protons were not detected upstream  
23 above our current sensitivity limit, but the incoming solar wind fluctuated in the foot  
24 region. We argue that the Jovian bow shock is not always in a steady state, and some of the  
25 observations might be connected with this fact. *INDEX TERMS:* 2784 Magnetospheric Physics:  
26 Solar wind/magnetosphere interactions; 2154 Interplanetary Physics: Planetary bow shocks; 2164  
27 Interplanetary Physics: Solar wind plasma; 2109 Interplanetary Physics: Discontinuities; *KEYWORDS:* Cassini,  
28 fields and particles, Jupiter, bow shock, solar wind parameters

29 **Citation:** Szego, K., et al., Cassini plasma spectrometer measurements of Jovian bow shock structure, *J. Geophys. Res.*, 108(0),  
30 XXXX, doi:10.1029/2002JA009517, 2003.

## 32 1. Introduction

33 [2] The objective of this paper is to report the first results  
34 on the properties of the Jovian bow shock as observed during  
35 the flyby of the Cassini spacecraft. The results presented  
36 here are based on the data collected by the magnetometer,  
37 radio and plasma wave science instrument (RPWS), and the  
38 Cassini plasma spectrometer (CAPS) carried on board Cas-

sini. The uniqueness of this data set is due to the favorable 39  
spacecraft orbit near Jupiter: in contrast to previous missions 40  
it skimmed the bow shock rather than crossing it quickly, and 41  
the craft spent a relatively long time in the different plasma 42  
regions close to it. More than forty bow shock crossings 43  
were recorded along the spacecraft orbit starting from the 44  
dayside and extending to the distant flank over more than 45  
three months. This allows the study of the giant Jovian bow 46  
shock under very special conditions, during high solar 47  
activity, not attained by other missions. 48

[3] Six spacecraft visited Jupiter before Cassini: Pioneer 49  
10 and 11, Voyager 1 and 2, Ulysses, and Galileo. With the 50  
exception of Galileo, these spacecraft arrived at the planet 51  
between 1000 and 1100 local time (LT), the first four left it 52  
between 0200 and 1200 LT and explored the dawnside of 53  
the Jovian bow shock (that is, the other side than Cassini). 54  
Owing to the strong corotation of the Jovian magneto- 55  
sphere, symmetry between the dusk/dawn sides cannot be 56  
taken for granted; therefore the Cassini data provide new 57  
information on the Jovian bow shock. 58

[4] Both Voyagers observed multiple inbound (between 59  
 $\sim 100$ – $\sim 60 R_J$  around 1100 LT) and outbound bow shock 60

<sup>1</sup>KFKI Research Institute for Particle and Nuclear Physics, Budapest, Hungary.

<sup>2</sup>Southwest Research Institute, San Antonio, Texas, USA.

<sup>3</sup>Los Alamos National Laboratory, Space and Atmospheric Science Group, Los Alamos, New Mexico, USA.

<sup>4</sup>Centre d'Étude des Environnements Terrestre et Planétaires, IPSL, France.

<sup>5</sup>Mullard Space Science Laboratory, University College London, London, UK.

<sup>6</sup>Imperial College, London, UK.

<sup>7</sup>Department of Physics and Astronomy, The University of Iowa, Iowa City, Iowa, USA.

crossings (between  $\sim 220$ – $\sim 280 R_J$  along the flank). Comparing these locations with the position of magnetopause crossings, *Scarf et al.* [1981] noted that the location of the boundaries vary widely in response to the presumed changes in the solar wind pressure and suspected that other causes may also play a role (such as interplanetary events). *Scudder et al.* [1981] reported a nearly perpendicular inbound shock for Voyager 1 with abrupt, near maximal ( $\sim 4$ ) density jumps, and a  $\sim 10$  electron temperature jump. (During that particular crossing the SW bulk velocity was  $\sim 400$  km/s, electron density  $\sim 0.5$  electron  $\text{cm}^{-3}$ ,  $T_e/T_p = 2.5$ , and  $\beta \sim 2$ . The core SW electron temperature was  $\sim 3$  eV, with a suprathermal component  $T_e \sim 43$  eV and 4% of core density). The plasma wave measurements [*Scarf et al.*, 1981] found intense broadband turbulences in a thin layer of the shock, preceded by intense bursts of electron plasma oscillations upstream. The outbound bow shock crossings were frequently weak and diffuse in the wave data, though still clearly identifiable. The Voyager observations confirmed that the Jovian magnetosphere is easily compressible.

[5] The Ulysses inbound shock was quasi-parallel ( $36^\circ$ ) at  $113 R_J$ , and three quasi-perpendicular crossings were detected outbound between  $109$  and  $149 R_J$  [*Balogh et al.*, 1992]. The Ulysses Radio and Plasma Wave experiment [*Stone et al.*, 1992] confirmed the presence of electrostatic bursts in the frequency range between  $10$  Hz and  $10$  kHz with the largest amplitude near the ramp. The solar wind plasma experiment [*Bame et al.*, 1992] detected at the inbound shock crossing a jump in electron density from  $0.06$  to  $\sim 0.15 \text{ cm}^{-3}$  and a temperature jump from  $\sim 0.2$  eV to  $\sim 1.5$  eV.

[6] *Kivelson et al.* [1997] compared the Galileo crossings with the results of the other missions. They concluded that the Jovian magnetosphere can experience large changes in its magnetic configuration and attributed it to the changes of the solar wind dynamic pressure.

[7] On the basis of the bow shock crossing locations of these missions, *Huddleston et al.* [1998] were the first who attempted to find an average shape of the Jovian bow shock. They have also pointed out the variability of the shock front due to the rapidly changing magnetodisk of Jupiter. None of the published papers discussed the details of the shock structure.

[8] Hybrid simulations of high Mach number bow shocks [*Leroy et al.*, 1982; *Quest*, 1985] indicated that shocks above a (second) critical Mach number ( $>13$ ) cannot be stationary; neither conventional energy dissipation mechanisms nor additional dissipation due to the reflected ions provide adequate dissipation required for a steady state. This, for instance, may lead to a nonstationary situation and may cause fluctuations, e.g., in the reflected particle distributions. In these papers it was also suggested that observations at Jupiter might help to resolve this issue.

[9] Several papers were published to describe the physics of the foot region of the shock [see, e.g., *Moses et al.*, 1985, and references therein], but as we shall discuss the CAPS foot observations in a separate paper, we do not go into details here.

[10] The goals of this paper are threefold: (1) to provide a phenomenological description of the Jovian bow shock in a region that has not been investigated previously, (2) to contribute to the analysis of the variability of the Jovian

bow shock, and (3) to discuss a few particular questions specified later. Most of the bow shock crossings we observed do not follow simple patterns, and at this point it is beyond our understanding to explain all the details of the plasma structures detected. In this paper only a part of the observations presented are interpreted. However, by selecting a few representative examples we would like to provide material for further studies by other teams as well.

[11] In the next section we describe the instrumentation used for data acquisition, Section 3 summarizes the solar wind conditions during the flyby; the two subsequent sections are devoted to describe bow shock properties, and we present our summary and conclusions in the last section.

## 2. Instrumentation

[12] The Cassini spacecraft, launched to study the environment of Saturn, flew by Jupiter on its way to tap the planet's gravity field. The closest approach took place on 30 December 2000. The CAPS instrument has three independently operated sensors: the ion mass spectrometer (IMS) designed to analyse ion composition and plasma dynamics, the electron spectrometer (ELS), and the ion beam spectrometer (IBS) to measure narrow, beam-like distributions without mass separation. CAPS is described in detail by *Young et al.* [1998, 2002]. The magnetometer (MAG) has several modes of operation; we use here 1-s or 4-s resolution data, depending on telemetry rate [see *Dougherty et al.*, 2002]. The radio and plasma wave science instrument (RPWS) [*Gurnett et al.*, 2002a, 2002b] acquires amplitudes of wave electric fields from approximately  $1$  Hz to  $16$  MHz and wave magnetic fields from approximately  $1$  Hz to  $12$  kHz providing a spectrum once per  $32$  to  $64$  seconds, depending on the instrument mode. The RPWS uses three monopole electric antennas and a set of triaxial search coils for sensors. For selected intervals, higher resolution observations are made with wideband and waveform receivers; however, such measurements are not included in this paper.

[13] During its flyby at Jupiter, Cassini performed complex scientific observations which required frequent changes in the spacecraft orientation; therefore the solar wind was not always in the field of view of CAPS (ELS sees the solar wind as the thermal velocity is higher for electrons), and instrument telemetry modes also varied. In this paper we report results from periods when the plasma flow was in the field of view of CAPS both before and after the bow shock crossings, and the telemetry rate for CAPS was  $2$  kbps. In this telemetry mode CAPS-IMS resolves energy in  $64$  logarithmic steps between  $1$  eV and  $50$  keV and elevation in four equal,  $40^\circ$  wide angular channels; one such spectrum was collected in  $16$  s. For CAPS-ELS [*Linder et al.*, 1998] the  $64$  logarithmic energy steps are between  $1$  eV and  $30$  keV, the  $160^\circ$  elevation field of view is split into  $20^\circ$  wide angular channels, and one such spectrum was collected in every  $32$  s (it is the modes used for many of the crossings which degrades the time resolution from the basic  $2$  s for an ELS sweep). The ion beam spectrometer, CAPS-IBS, has three entrance apertures offset by  $30^\circ$ , and each field of view is  $1.5^\circ \times 150^\circ$ . CAPS-IBS collected all ions in  $256$  specially selected narrow energy steps between  $\sim 200$  eV and  $\sim 9.5$  keV with energy resolution  $\Delta E/E =$

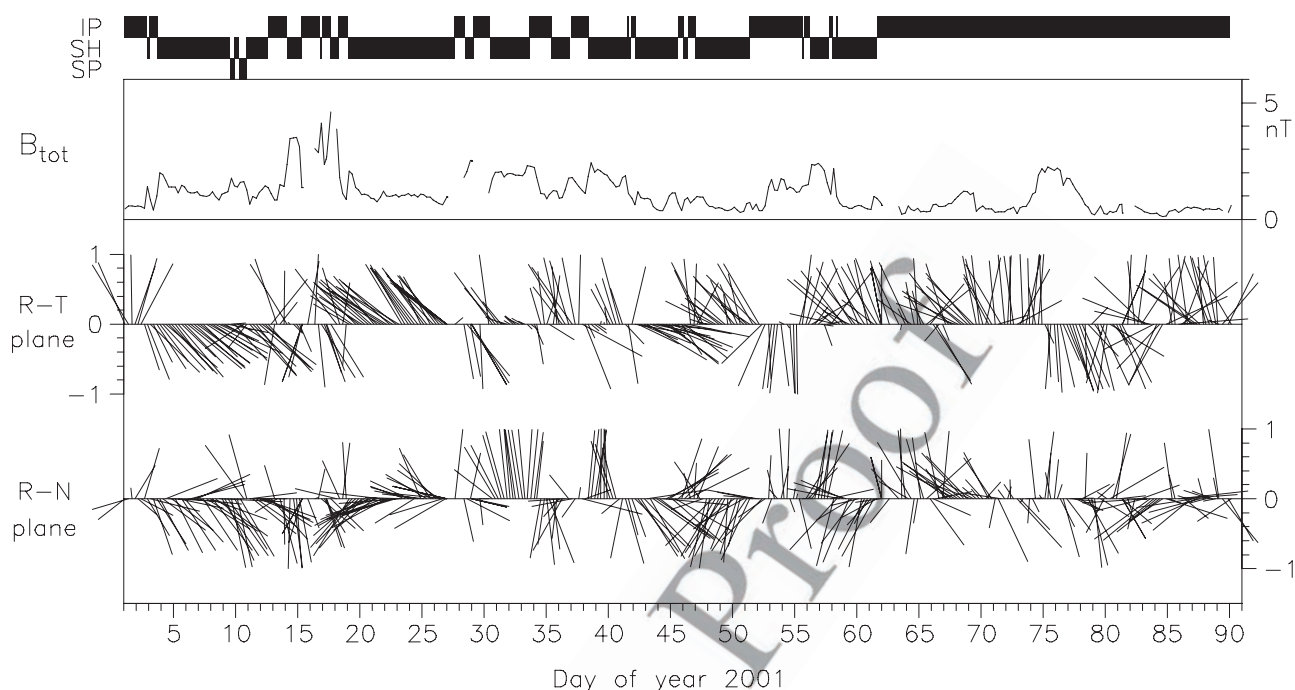


**Figure 1.** Six-hours averaged magnetic field vector directions are shown in the RTN frame of reference, as measured by the magnetometer onboard Cassini in 2001, between DOY 001 and 090. The approximate time of the bow shock crossings are shown in the upper plot (W. S. Kurth et al., private communication, 2002), the abbreviations denote the different plasma regions: IP = interplanetary (upstream), SH = magnetosheath, SP = magnetosphere. Below the magnitude of the magnetic field is displayed; then the field vector directions in the R-T ( $\sim$ close to the Solar ecliptic plane) and R-N planes are shown.

183 0.015; one full spectrum was taken in 0.5 s. In the 2 kbps  
 184 telemetry mode, 16 sweeps were added during a 32-s long  
 185 time interval. The field of view in the azimuth direction was  
 186  $11^\circ$  for IMS,  $5^\circ$  for ELS, and  $1.5^\circ$  for IBS. The whole CAPS  
 187 package can be actuated around a rotation axis parallel to  
 188 the symmetry planes of the IMS and ELS field of views and  
 189 oriented perpendicular to the symmetry axes of these instru-  
 190 ments FOV.

191 [14] The actuator performed windshield-wiper-like mo-  
 192 tion in a variable-length interval, the highest angular veloc-  
 193 ity being about  $1^\circ \text{ s}^{-1}$ ; the actuator-plane position defines  
 194 the azimuth plane of the look direction (the actuation is in  
 195 X-Y plane in the spacecraft coordinate system;  $0^\circ$  azimuth  
 196 corresponds to viewing out along the Y axis of the space-  
 197 craft coordinate system). In the 2 kbps telemetry mode,  
 198 azimuth values were summed for IMS during a 16-s long  
 199 time interval, for ELS and IBS in a 32-s long interval; this is  
 200 the best time/space resolution in this mode of operation. In  
 201 the solar wind (SW), however, if the plasma flow was stable  
 202 for a longer period of time, even a few-degree azimuth  
 203 resolution could be achieved during multiple scans exploit-  
 204 ing the fact that the actuator motion is not in phase with the  
 205 data acquisition time-interval. A detailed description of IBS  
 206 operation was published by *Vilppola et al.* [2001].

### 207 3. Solar Wind at Jupiter, Global Features

208 [15] Cassini encountered Jupiter during a period of high  
 209 solar activity, and according to the investigators of the

magnetometer onboard Ulysses, two magnetic sectors were 210  
 present on the Sun up to high latitudes in the year 2000 and 211  
 at the beginning of 2001 [*Smith et al.*, 2001]. The picture 212  
 emerging from this appears to be consistent with a single 213  
 warped current sheet tilted slightly to the rotation axis of the 214  
 Sun. The 6-hour averaged magnetic field vectors in the RTN 215  
 coordinate system for the first 90 days of 2001, shown in 216  
 Figure 1, indicate very dynamic magnetic field variations, 217  
 and the out-of-ecliptic field components (N-direction) were 218  
 frequently high. (The RTN coordinate system is defined as 219  
 follows: the R unit vector points from the Sun to the 220  
 spacecraft direction, the T unit vector points to the  $\Omega \times \mathbf{R}$  221  
 direction where  $\Omega$  is the Sun spin axis, and the N unit vector 222  
 completes the right-hand system. When R is in the ecliptic 223  
 plane, N is almost parallel to the ecliptic north, the differ- 224  
 ence being less than  $8^\circ$ . On DOY 055 and DOY 075 a 225  
 sector boundary crossing is evident from the sudden change 226  
 of the field components in the ecliptic plane, and the relative 227  
 stability of its direction between these dates. Large-scale 228  
 structures with a relative stability of the direction of the IMF 229  
 in the ecliptic plane can also be found between days 3 and 230  
 13, 17 and 27. 231

[16] The “nominal” solar wind parameters at Jupiter are 232  
 $B \sim 1.2 \text{ nT}$ ,  $n \sim 0.3\text{--}0.4 \text{ particle cm}^{-3}$ ,  $v \sim 400 \text{ km/s}$ , the 233  
 Parker spiral angle between the SW velocity and the 234  
 magnetic field vector being  $\sim 79^\circ$  (see, e.g., chapter 6.4.2 235  
 of *Cravens* [1997]). We derived the 1-hour averaged solar 236  
 wind velocity vectors by fitting a Maxwellian distribution to 237  
 all IMS data points. Because the actuator did not move in 238

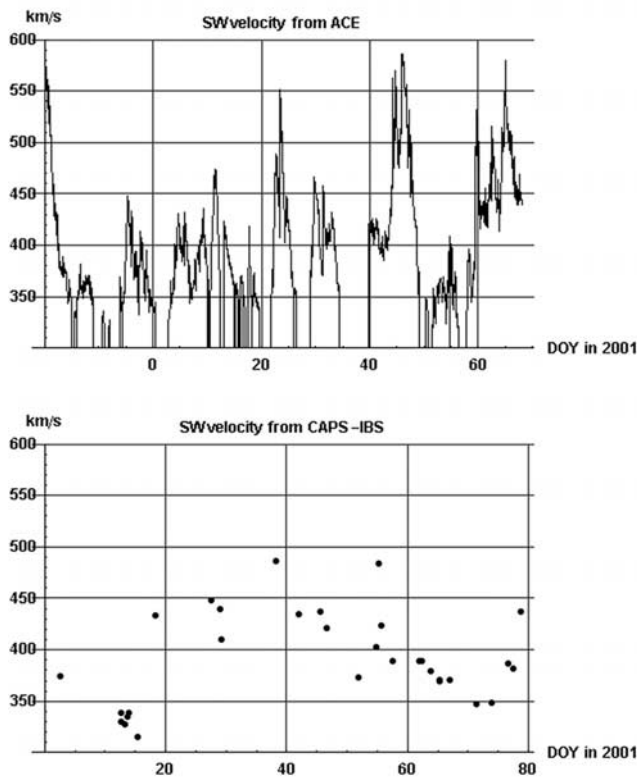


**Figure 2.** The variation of the 1-hour averaged SW velocity at Jupiter during the first 80 days of 2001 based on 2 kbps IBS data (lower panel) and at Earth starting 20 days earlier using the SWEFAM instrument data onboard ACE (upper panel).

239 phase with the data collection time interval, this allows a  
 240 relatively accurate determination of the x and y components  
 241 of the SW velocity in the spacecraft frame of reference if the  
 242 SW is stable. As we have mentioned, the resolution along  
 243 the spacecraft z-direction was coarse ( $40^\circ$ ); therefore the  
 244 z-component of the velocity vector in the spacecraft coordi-  
 245 nate system has much higher error than the two other  
 246 components. The 1-hour averaged total velocity of the SW  
 247 was also derived from the IBS data. These values are plotted  
 248 in Figure 2. In the same figure we have also exhibited the  
 249 SW velocities at Earth, as obtained by the SWEFAM  
 250 instrument onboard ACE, publicly available from  
 251 [www.srl.caltech.edu/ACE/](http://www.srl.caltech.edu/ACE/). This supports earlier recom-  
 252 mendations [Huddleston et al., 1998] that with appropriate  
 253 time shift the SW parameters measured at the Earth can be  
 254 used as proxy if needed because the Earth and Jupiter were  
 255 almost aligned during this period.

256 [17] We have two methods to obtain the SW temperature.  
 257 One is to fit Maxwellians to the IBS energy distribution.  
 258 The second is to exploit the azimuth extent of the plasma  
 259 distributions. Assume that the SW distribution can be  
 260 described by a Maxwellian centered on the bulk velocity  
 261 vector  $\{v_x, v_y, v_z\}$  with  $v_T$  as half-width, where  $v_T$  is the SW  
 262 thermal velocity. To take into account the smearing effect of  
 263 the  $11^\circ$ -wide field of view of the IMS sensor in azimuth, we  
 264 convolute the instrument response function with the SW  
 265 distribution in the azimuth direction (but not in elevation  
 266 direction because the FOV resolution in elevation is wider

than the angular distribution of the solar wind ions). With  
 good enough accuracy, the azimuth response function can  
 be approximated by a Maxwellian centered on the actual  
 view direction, with half width  $|v_{\text{bulk}}| \tan(3^\circ)$ . The convo-  
 lution of two Maxwellian is again a Maxwellian with a  
 modified thermal velocity  $v_{T,\text{mod}} = (v_T^2 + v_{\text{bulk}}^2 \tan^2(3^\circ))^{1/2}$ .  
 Therefore the SW temperature was obtained by integrating  
 the counts over  $v_z$  and  $(v_x^2 + v_y^2)^{1/2}$ , assuming a Maxwell-  
 ian distribution function with  $v_{T,\text{mod}}$  in the x-y directions.

$$\int v dv \int dv_z \frac{1}{\pi^{3/2} v_{T,\text{mod}}^3 v_T} \exp\left[-\frac{(v_z - v)^2}{v_T}\right] \cdot \exp\left[-\frac{((v \cos \varphi - v_{x0})^2 + (v \sin \varphi - v_{y0})^2)}{v_{T,\text{mod}}^2}\right] = \frac{1}{2\pi} [\exp(-\alpha^2) + \exp(-\alpha^2 \sin^2(\varphi_{\text{max}} - \varphi))] \cdot \sqrt{\pi} \alpha \cos(\varphi_{\text{max}} - \varphi) [1 + \text{erf}(\alpha \cos(\varphi_{\text{max}} - \varphi))]$$

where  $\alpha = \frac{\sqrt{v_{x0}^2 + v_{y0}^2}}{v_{T,\text{mod}}}$ , and  $\varphi_{\text{max}} = \text{arc cos}\left(\frac{v_{y0}}{\sqrt{v_{x0}^2 + v_{y0}^2}}\right)$ .

[18] Then using the calculated  $v_{x0}$  and  $v_{y0}$  velocity components, we fitted an overall scale factor and  $v_T$  to the integrated counts. An illustration of the SW temperature fit is shown in Figure 3. The temperature obtained this way is somewhat higher than the temperature obtained by fitting Maxwellian directly to the IBS data. Despite this small discrepancy (to be clarified in the future) we shall use both methods because it does not affect the observations presented in this paper.

[19] During the 3 month long interval shown in Figure 1 the solar wind exhibited high variability; the presence of

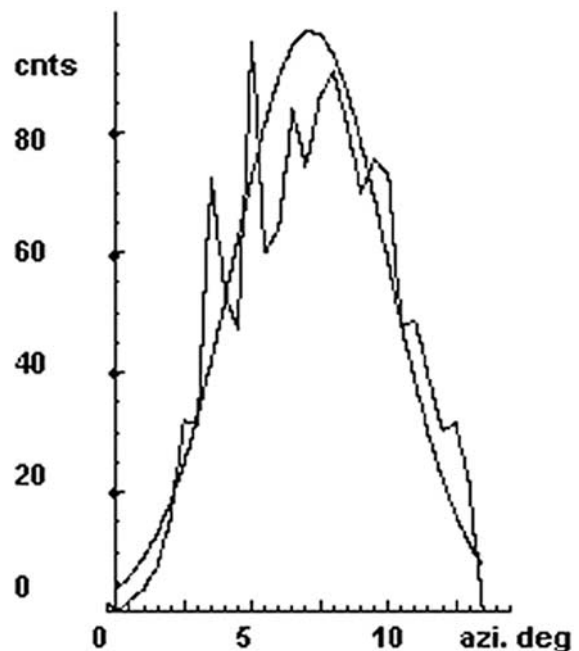


**Figure 3.** The count-azimuth distribution of the SW on DOY 012 between 1500 and 1600 UT. The horizontal axis is azimuth in degrees; the vertical axis displays counts. The fit corresponds to  $v_x = 257$  km/s,  $v_y = 127$  km/s, and  $v_{\text{bulk}} = 298$  km/s in the spacecraft frame of reference, and  $v_T \sim 12$  km/s.

289 small and mesoscale structures was evident in the flow,  
 290 including interplanetary shocks. We illustrate these by some  
 291 characteristic events. On DOY 002 and 003, before Cassini  
 292 crossed the bow shock, the magnitude of the SW velocity  
 293 was about 320–330 km/s, and the SW was cold, with  $v_T \sim$   
 294  $10 \div 12$  km/s. The structure of the shocked solar wind  
 295 between DOY 003 and 012 and the differences of the  
 296 boundary positions as measured by Galileo and Cassini  
 297 were interpreted by Hill [2002] as the effect of an inter-  
 298 planetary shock that passed Jupiter. At the end of the DOY  
 299 012, at about 2200 UT, the T and N components of the  
 300 magnetic field vector changed sign, and a hot SW stream  
 301 crossed the spacecraft, and  $v_T$  jumped to  $25 \div 30$  km/s  
 302 without any significant change in the magnitude of the  
 303 velocity. Cassini probably crossed another interplanetary  
 304 shock on DOY 015  $\sim$  1140 UT, shown in Figure 4, the SW  
 305 energy and temperature jumped up together, with a signif-  
 306 icant change in the magnetic field data. In the RPWS data  
 307 the IP shock is seen in the lower frequency range. Several  
 308 other IP shocks were seen during this 90 day long period of  
 309 time as well.

310 [20] The increase in SW velocity and temperature around  
 311 DOY 018 (cf., Figure 2) is probably the signature of a  
 312 sector boundary crossing. Between DOYs 040 and 060 the  
 313 magnetic field was fluctuating even in a 1-hour long scale,  
 314 and a sector boundary crossing is likely on DOY 055 (see  
 315 Figure 1). It seems likely that between DOYs 052 and 055,  
 316 Cassini was in the midst of hot SW. The SW became slower  
 317 and colder around DOYs 060 and became faster and hotter  
 318 close to the sector boundary crossing around DOY 075.

#### 319 4. Bow Shock on DOY 012

320 [21] Cassini encountered the Jovian bow shock first time  
 321 on 28 December 2000,  $\sim$ 0419 UT, but the first bow shock  
 322 crossing with full CAPS coverage took place on 12 January  
 323 2001,  $\sim$ 1420 UT, at a distance of about  $224 R_J$  ( $1 R_J =$   
 324  $71,492$  km) from the planet,  $\sim 24^\circ$  behind the terminator  
 325 line in the orbit plane, and the spacecraft was  $\sim 0.7^\circ$  below  
 326 the solar equatorial plane. During the time interval dis-  
 327 cussed here the CAPS instrument was actuated around an  
 328 axis perpendicular to the ecliptic plane, from  $-79^\circ$  to  $102^\circ$   
 329 in azimuth, the solar wind arrived from the  $56^\circ$ – $70^\circ$   
 330 azimuth interval in the spacecraft coordinate system. In  
 331 the RTN frame of reference the unperturbed SW velocity  
 332 was about  $v_{SW} = \{315, 14, 82\}$  km/s as derived from the  
 333 CAPS-IMS SW spectra measured between 1500 and 1600  
 334 UT when the wave activity was quiet. The variation of the  
 335 magnetic field vectors in RTN and the bulk plasma veloc-  
 336 ities as derived from IBS are shown in Figure 5.

337 [22] The shock crossing is evident from the steep jump of  
 338 the magnetic field at 1420 UT. In general the magnetic field  
 339 near the bow shock is seldom stable; therefore we describe  
 340 how we obtained the shock normal. Two methods were used  
 341 to determine the shock normal from the measured magnetic  
 342 field data. One is based on the coplanarity theorem, by  
 343 taking the upstream and downstream averages of the mag-  
 344 netic field vectors,  $\mathbf{B}_u$  and  $\mathbf{B}_d$  and calculating the shock  
 345 normal  $\mathbf{n}$  as the unit vector parallel to  $(\mathbf{B}_u - \mathbf{B}_d) \times (\mathbf{B}_u \times$   
 346  $\mathbf{B}_d)$  or else  $\mathbf{n} \cdot (\mathbf{B}_u \times \mathbf{B}_d) = 0$ . The other method used the  
 347 minimum variance technique. The normal is expected in the  
 348 plane perpendicular to the maximum variance direction.

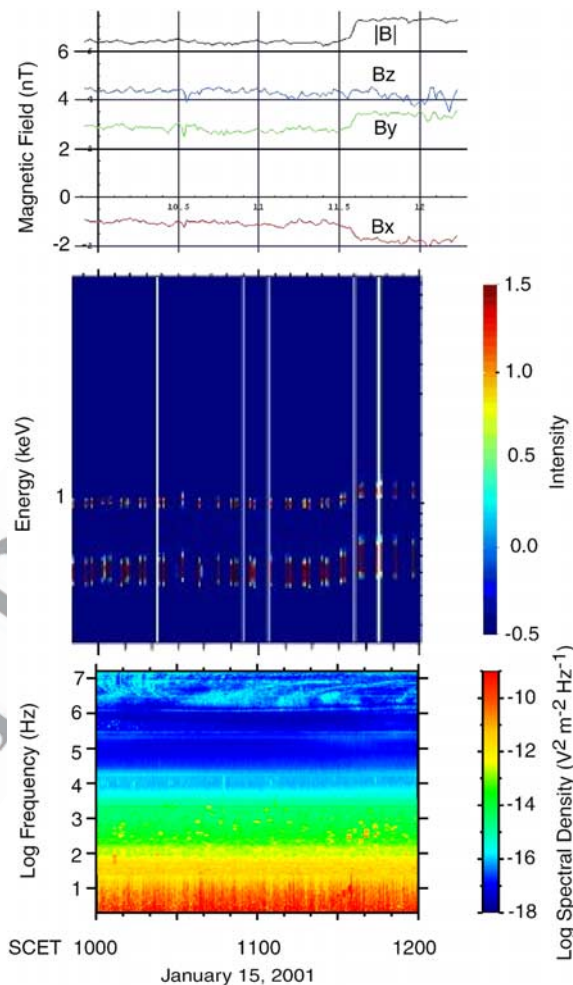


**Figure 4.** An interplanetary (IP) shock on DOY 015 between 1000 and 1200 UT. The upper plot shows the magnetic field components in the spacecraft frame of reference ( $B_x$  is red;  $B_y$  is green, shifted up by 2 nT;  $B_z$  is blue, shifted up by 4 nT) and the total field (black) shifted up by 5 nT. The middle plot shows the IBS energy spectra, whereas the lower plot exhibits the RPWS data for the same time interval.

The measured field vectors were projected to the plane, 349  
 and the normal was selected by taking the direction parallel 350  
 to the average of those vectors. In both methods the time 351  
 interval of the shock transition was discarded. 352

[23] Both methods give uncertain results close to either 353  
 quasi-parallel or to quasi-perpendicular shocks. Further, 354  
 there is a danger, especially with the variance technique, 355  
 that the calculation of normal can be misled by large 356  
 amplitude waves not associated with the shock transition. 357  
 We have checked the consistency of the calculation by 358  
 selecting various time intervals for the upstream, down- 359  
 stream, and shock transition regions. The normal is accept- 360  
 able if the two methods give similar results and which are 361  
 relatively insensitive for the selected time intervals. 362

[24] On DOY 012 the shock was quasi-perpendicular, 363  
 $\theta_{Bn} > 80^\circ$ , the shock normal in RTN pointed to  $\{-0.62,$  364  
 $-0.76, 0.18\}$ , so the spacecraft velocity was almost per- 365  
 pendicular to the shock normal, indicating that the space- 366

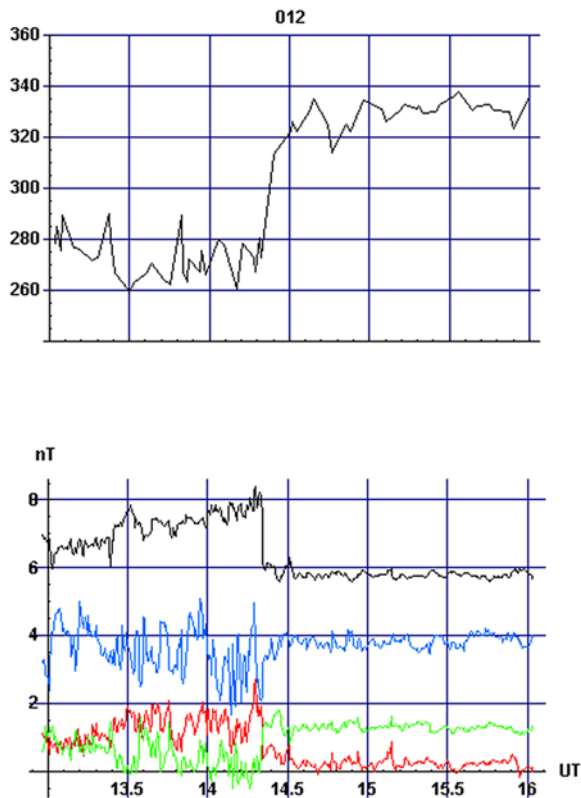


**Figure 5.** The upper plot shows the bulk plasma velocity on DOY 012 between 1300 and 1600 UT; the lower plot exhibits the magnetic field components in RTN for the same time period. The plot label contains the explanation of color coding and level shifts for the magnetic field components.

craft was really “skimming” the shock. Despite that, the crossing was very fast; according to the hi-res magnetic data, the spacecraft crossed the shock ramp in 8 s. The shock normal direction for this crossing agrees reasonably well with the shape model of *Huddleston et al.* [1998].

[25] In the wave data the signature of this bow shock crossings is very clear: it is a sharp signal outstanding in the proton plasma frequency region ( $f_p = 210 n^{1/2}$  Hz), extending up to 1000 Hz. Similar wave signature in the ramp was observed during the Voyager mission as well [*Moses et al.*, 1985; *Scarf et al.*, 1987]; it is believed that this is due to electrostatic ion waves [*Wu et al.*, 1984]. The characteristics of this signal are not different from the one observed at Earth by RPWS on Cassini [*Moses et al.*, 1990; *Kurth et al.*, 2001]. This is a good example that certain shock features are independent of the obstacle. The shock is also clearly seen in the CAPS-IBS data: the ion thermalization downstream is an excellent signature of bow shock crossings. These are illustrated in Figure 6, showing the IBS energy spectra together with the wave data measured in the same time interval.

[26] The wave spectra seen in Figure 6 show intense peaks upstream around 10 kHz; we identify those with Langmuir waves. From these and also from the IBS spectra an approximate upstream density of about  $0.5 - 1 \text{ cm}^{-3}$  is obtained. The upstream electron temperature, as derived from the SW electron spectra, was about 2.6 eV. Using the measured  $B_{\text{tot}} \sim 0.8 \text{ nT}$  shown in Figure 5, we get  $v_A \sim 32 \text{ km/s}$ ;

hence the SW Mach number was  $M_A \sim 10$  (for the velocity component perpendicular to the bow shock  $M_A \sim 7$ ). The spacecraft velocity was  $\{9.3, -5.1, 0.6\} \text{ km/s}$  in RTN. According to hybrid simulations [*Leroy et al.*, 1982], the width of the foot of quasi-perpendicular shocks is about the proton gyroradius,  $\sim 1500 \text{ km}$  for the nominal SW parameters, and the shock width is about the proton’s inertial length,  $\sim 300 \text{ km}$ . We conjecture from this sharp transition that in this period the shock ramp passed over the spacecraft with a  $\sim 30 \text{ km/s}$  velocity.

[27] Four downstream ion distributions are shown in Figure 7 as a function of velocity. Thermalization increases farther from the shock front (the distribution “1” is the farthest); the change in the peak velocity is significant but does not show a clear trend. The presence of a non-Maxwellian tail is evident even from visual inspection of the data. Note the absence of a downstream shoulder, typically seen in Earth’s magnetosheath, due to reflected ions.

[28] We have solved the Rankine-Hugoniot relations for this transition (being aware that this is only an approximation for the plasma flow we investigate), using the measured upstream parameters and the measured downstream magnetic field values. This yields for the downstream plasma parameters  $\rho_{\text{down}}/\rho_{\text{up}} \sim 2.74$ ,  $v_{\text{down}} = \{233, -66, -96\} \text{ km/s}$  equivalent to a downstream bulk energy  $\sim 360 \text{ eV}$ , and a bulk velocity  $\sim 260 \text{ km/s}$ , agreeing reasonably well with the data shown in Figure 7. For the total downstream plasma temperature the R-H conditions predict 44 eV. The downstream electron temperature from ELS data is about 11 eV, leaving  $\sim 33 \text{ eV}$  for the downstream ion temperature. The proton temperature can be assessed also from the azimuth extent of the distribution, yielding  $\sim 24 \text{ eV}$ , as can be seen

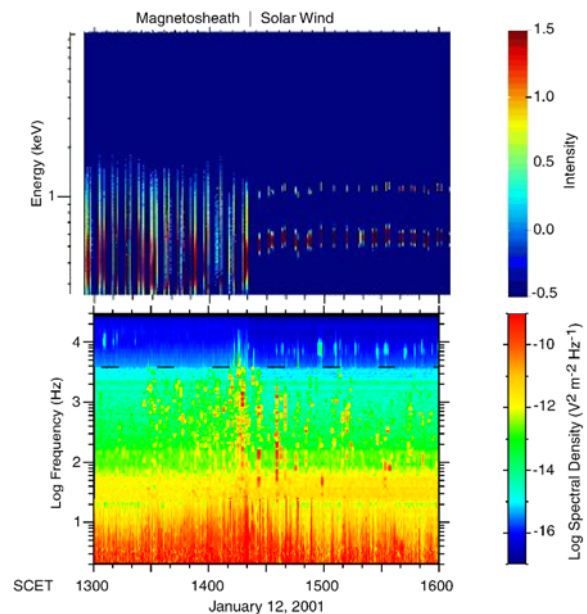


**Figure 6.** The upper plot displays the IBS counts on DOY 012 between 1300 and 1600 UT; time is shown on the horizontal axis. The vertical axis is energy in log eV; color represents log count number marked as “intensity.” The lower plot is the wave spectrum for the same time interval, measured by RPWS. The vertical axis shows wave frequency; color is wave intensity.

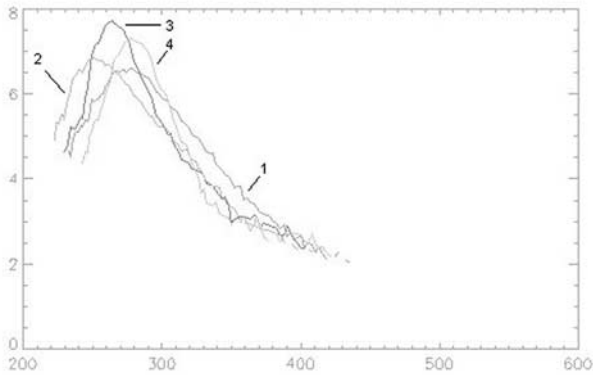


**Figure 7.** IBS ion log-distributions as a function of velocity measured downstream at 1403 UT (between actuator angles  $31^\circ$  and  $64^\circ$ ) (1), 1410 UT ( $39^\circ$ – $71^\circ$ ) (2), 1417 UT ( $47^\circ$ – $79^\circ$ ) (3), and 1419 UT ( $50^\circ$ – $83^\circ$ ) (4). The horizontal axis displays velocity in km/s. The BS crossing took place at  $\sim 1420$  UT.

also in Figure 7. The angle between the upstream and downstream velocities is about  $18^\circ$ ; this agrees reasonably well with the  $20^\circ$  velocity deflection derived from actuator motion. The plasma motion obtained from the R-H relations reproduces quite well the observed bulk behavior downstream.

[29] It is more difficult to understand why we did not detect particles reflected back from the shock front. Both the flyby geometry and the FOV of the CAPS IMS and IBS sensors would have allowed to detect specularly reflected particles (in the vicinity of  $-30^\circ$  actuator angle) or particles streaming along the upstream magnetic field (in the  $-30^\circ$ – $0^\circ$  actuator range) but upstream no single count was detected outside the SW flow direction; also we do not see downstream shoulder. On the other hand, other evidences strongly suggest their existence:

[30] 1. The lower hybrid waves shown in Figure 6 in the foot region are very likely excited by reflected ions; especially intense waves are seen between 1430 and 1440 UT, 1500 and 1510 UT, and 1530 and 1540 UT.

[31] 2. The deceleration of the SW between the shock ramp and 1435 UT is very likely due to the increased ion population in the foot.

[32] One possible explanation, supported by test particle simulations, is that the reflected particles expand very quickly in phase space, both in the configuration and in the velocity space resulting in a flux below our sensitivity threshold. The intensive lower hybrid waves heat the incoming SW; such a heating is evident in Figure 6 around 1440 UT and 1540 UT as well. Even in these cases we did not see direct evidence of back-scattered particles.

[33] A related question is the observation of particles accelerated at the shock front. Shock acceleration processes, e.g., shock surfing, and shock drift acceleration were compared using a hybrid code for quasi-perpendicular shock by *Lever et al.* [2001]. Although in that study the incoming flow was a pickup ion shell, the conclusions are applicable to this case as well. An important conclusion was that the type of the acceleration mechanism for any given particle is defined by the kinetic parameter values valid at

the first encounter of the given particle with the bow shock. Whereas accelerated and reflected particles were not seen upstream by CAPS, we believe that the high energy tail of the ion distributions downstream, shown in Figure 7, is due to ions accelerated at the shock front. These ions lose energy while crossing the shock ramp due to the anomalous resistivity resulting from wave-particle interaction [cf., *Leroy et al.*, 1982], but they reach the downstream region with energies still exceeding the upstream SW energy. Comparing to the velocity gains obtained by those simulations, the gains we detected are modest. Shock surfing leads to high velocities, and it is effective for narrow foot and low incoming velocity; therefore we conclude that shock surfing was not dominant at this crossing.

[34] Magnetic waves are seen superimposed on the shock. The wave structure is more clearly seen if we plot the endpoints of the magnetic field vectors in the system of reference where the shock transition is parallel to the x-axis. This is shown in Figure 8. The  $B_y$ – $B_z$  hodogram indicates linear polarization in the downstream region.

## 5. Bow Shock on the Flanks

[35] In this section we discuss four other bow shock crossings, on DOY 042 between 0430 and 0500 UT inbound, on DOY 045 between 1400 and 1430 UT outbound, on DOY 055 between 1400 and 1430 UT inbound and  $\sim 1630$  outbound, and on DOY 057 around 1430 UT; at a distance of 576, 618, 744, and 770  $R_J$ , and at angles  $47.5^\circ$ ,  $48.3^\circ$ ,  $49.8^\circ$  and  $50^\circ$  behind terminator, respectively. For these bow shock crossings, the IBS energy-time spectra, the bulk plasma velocity, the magnetic field vectors, and the waves as measured by RPWS are shown in Figures 9–12, respectively.

[36] The shock crossings are evident by the onset of strong proton thermalization in the IBS energy-time spectra; in the RPWS this onset is always accompanied by a reasonably strong electrostatic signal, similar to the one shown in Figure 6. However, it would be very difficult to find the shock location only from the wave and magnetometer data. The variation of the bulk ion velocity shows a similar “smeared” picture; the quiet upstream and downstream regions are separated by hours.

[37] The solar wind velocities in RTN coordinates were (419,  $-88$ ,  $-93$ ), (407,  $-133$ , 16), and (404,  $-129$ , 6) km/s, respectively, for DOYs 042, 045, and 055; we could not derive the velocity vector for DOY 057 owing to the unfavorable spacecraft orientation. The Alfvén velocity for these days was  $\sim 22$  km/s,  $\sim 22$  km/s, and  $\sim 50$  km assuming 0.7 particle density per cc. (The density values were derived from the Langmuir waves; see section 4.) The large off-radial SW velocity components are to be noted; these are due to the relatively high z-component of the velocity in the spacecraft frame of reference. As the sampling in this direction (in the elevation direction) is coarse, these values might have been overestimated. The extent in azimuth of the upstream proton distributions were  $18^\circ$ ,  $18^\circ$ ,  $17^\circ$ , and  $18^\circ$ , respectively, leading to  $\sim 20$  km/s ( $\sim 4$  eV) thermal proton velocities upstream. On these days the SW was not fully in the CAPS field of view; a small portion of it (maximum  $5^\circ$ ) might have been missed at peak actuator angles. During the first three shock crossings the CAPS sensors were actuated

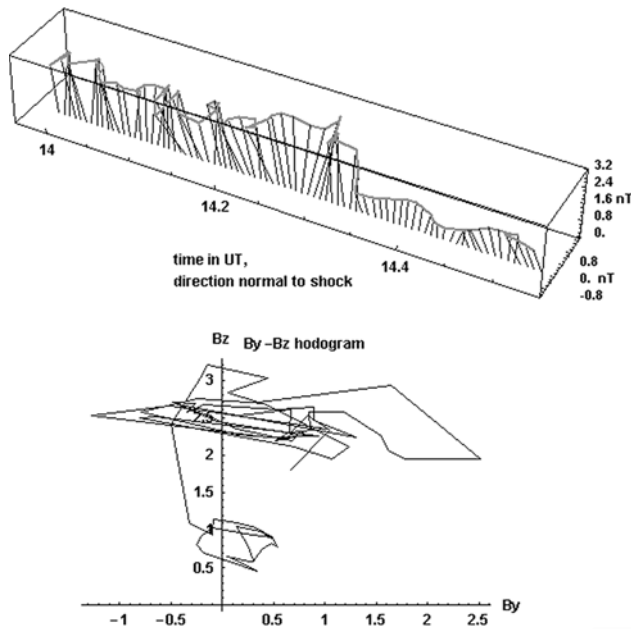


**Figure 8.** The upper plot shows the endpoints and directions of the magnetic field on DOY 012 between 1400 and 1433 UT. The magnetic field vectors are plotted as a function of time along the x-axis; this is the direction perpendicular to the shock front. The lower plot exhibits the hodogram in the  $B_y$ – $B_z$  plane for the same period of time; both axes show the field strength in nT.

527 between  $49^\circ$  and  $102^\circ$ , and for the last one they were  
 528 actuated between  $-79^\circ$  and  $101^\circ$ . We attempted to correct  
 529 the count rates by adding the missing values symmetrically  
 530 to the distribution functions, but these did not change  
 531 significantly either the SW velocities given above or the  
 532 temperature data.

533 [38] We derived the shock normal direction from the quiet  
 534 intervals before and after the perturbed regions a few hours  
 535 apart (this is an uncertain method because the SW shown in  
 536 Figure 2 does not support the assumption that it was quiet  
 537 for hours). The shock on DOY 042 was parallel ( $\theta_{Bn} \sim 2^\circ$ ,  
 538  $\mathbf{n}_{RTN} \sim \{-0.94, 0.3, 0.2\}$ ); the overall shape of the  
 539 magnetic field supports this conclusion; this shock is a  
 540 typical parallel turbulent shock transition. For DOY 045 we  
 541 have ( $\theta_{Bn} > 70^\circ$ ,  $\mathbf{n}_{RTN} \sim \{-0.3, 0.5, -0.8\}$ ). The shock on  
 542 DOY 055 was oblique ( $\theta_{Bn} \sim 50^\circ$ ,  $\mathbf{n}_{RTN} \sim \{-0.4, -0.8,$   
 543  $0.3\}$ ) outbound and quasi-parallel inbound. On DOY 057  
 544 we had ( $\theta_{Bn} \sim 70^\circ$ ,  $\mathbf{n}_{RTN} \sim \{-0.1, -0.7, 0.7\}$ ). These  
 545 yields as perpendicular Mach numbers (the ratio of the SW  
 546 velocity perpendicular to the shock and  $v_A$ )  $\sim 18$  for DOY  
 547 042 and  $\sim 9$  for DOYs 045 and 055. From the known

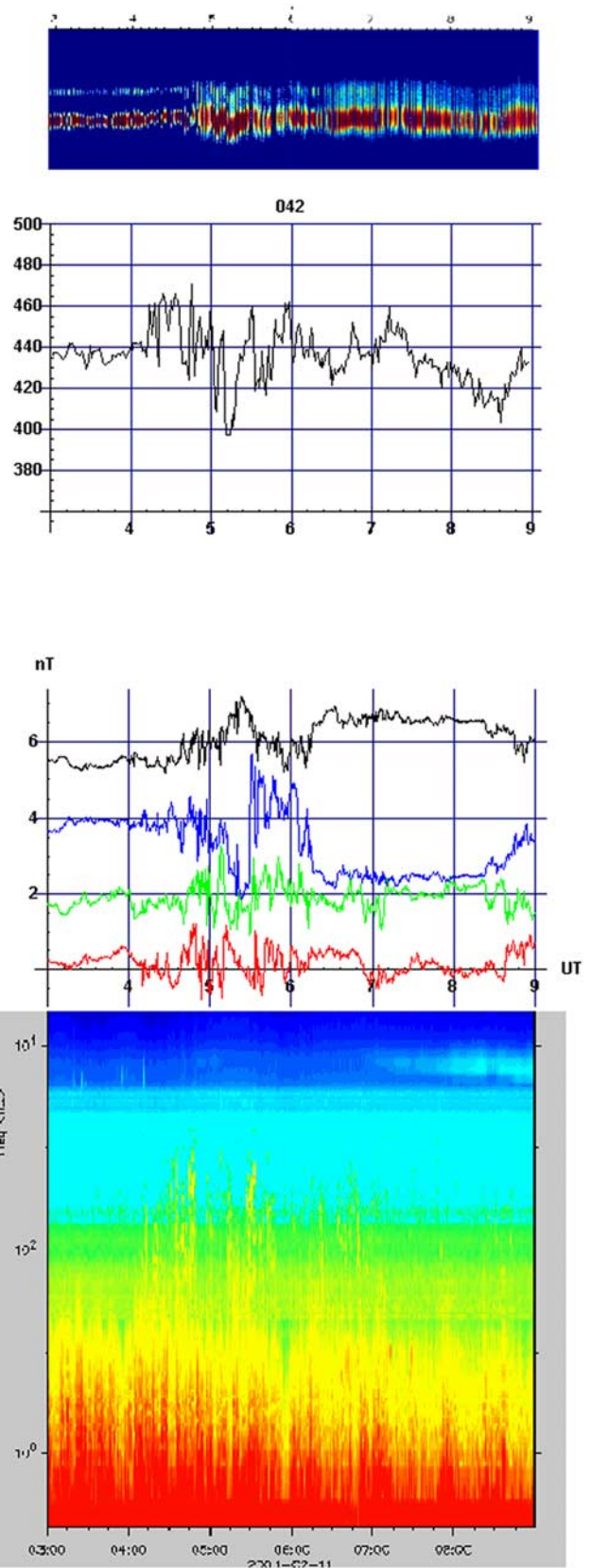


**Figure 9.** (opposite) A compilation of the plasma parameters for DOY 042, 0300–0900 UT. All horizontal axes show time in UT. The top panel shows the IBS energy spectra; the color code and scale are the same as shown in Figure 6. The top middle panels exhibits the bulk plasma velocity; the vertical scale is in km/s. The lower middle panels show the magnetic field data; the notations are the same as in Figure 4. The lower panel exhibits the wave data; the color scale is the same as in Figure 6.



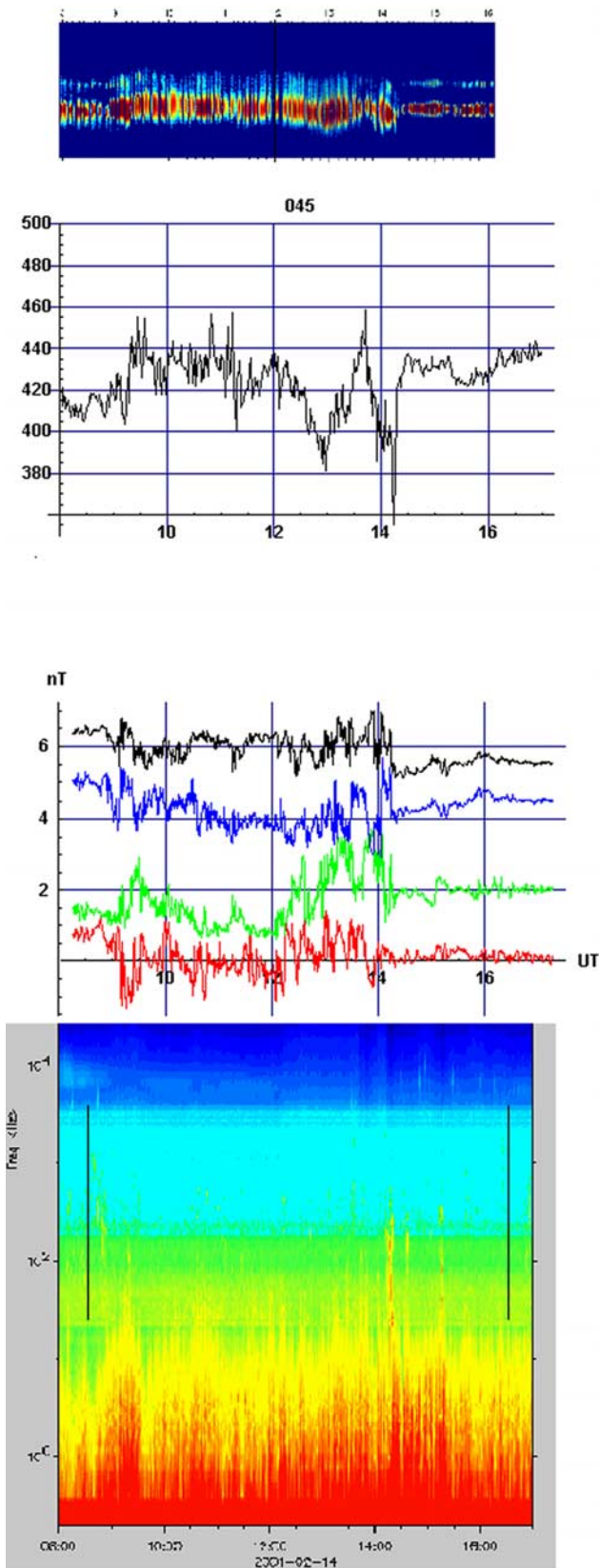


**Figure 10.** A compilation of the plasma parameters for DOY 045, 0800–1700 UT. The notations are the same as in Figure 9.

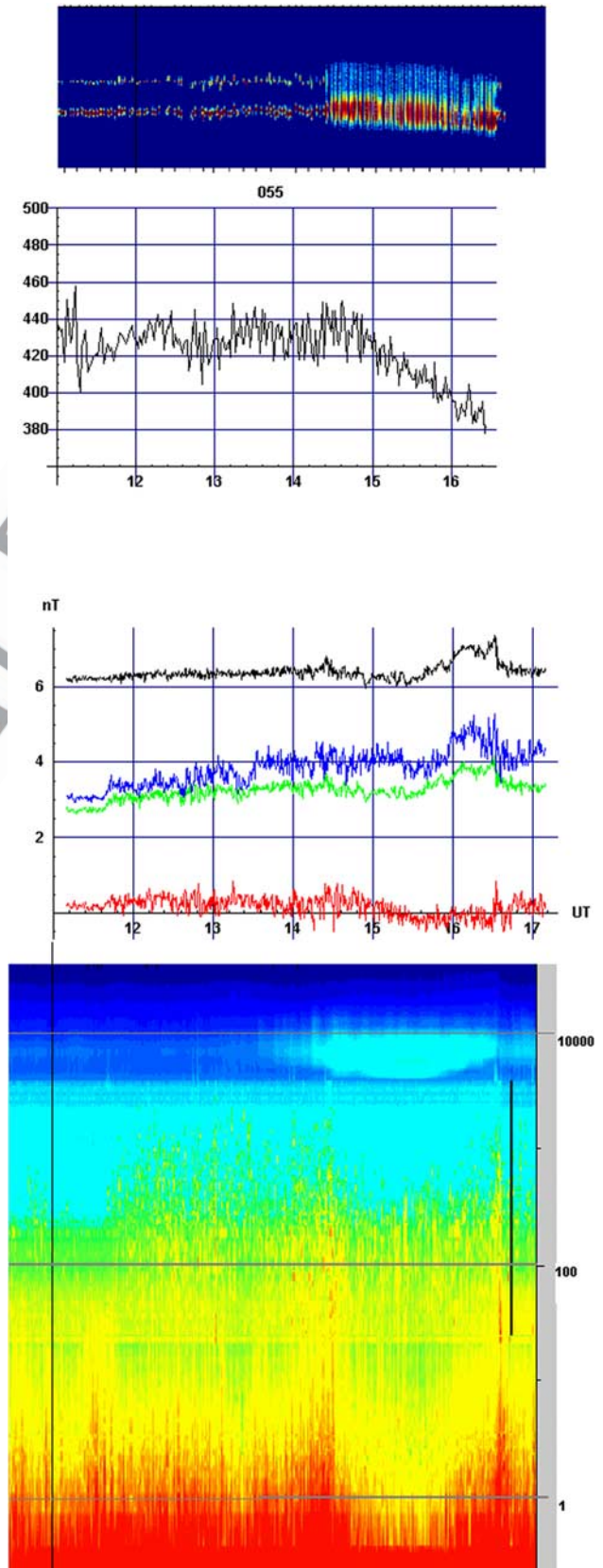
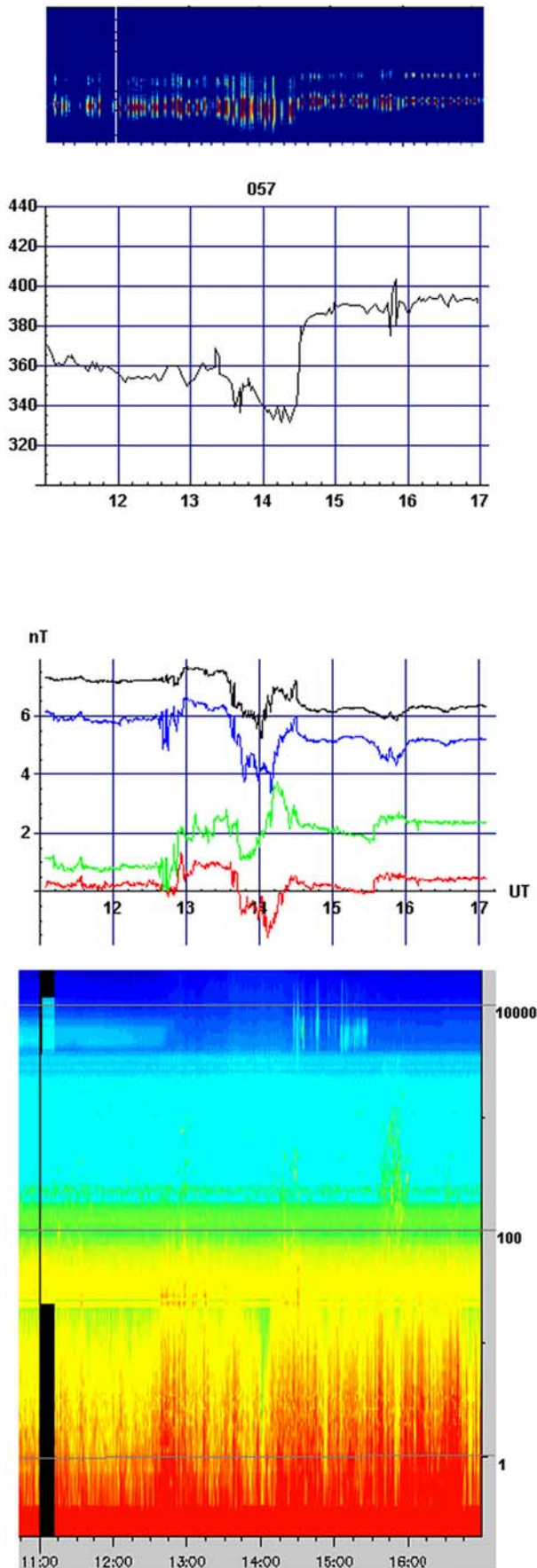


**Figure 11.** A compilation of the plasma parameters for DOY 055, 1000–1700 UT. The notations are the same as in Figure 9.



spacecraft velocity it is easy to calculate the angles between 548  
the spacecraft velocity vectors and the shock normals, these 549  
are  $169^\circ$ ,  $124^\circ$ ,  $83^\circ$ , and  $70^\circ$ , respectively. 550

[39] Many features of these shock transitions are beyond 551  
our understanding. On DOY 042 we expect strong wave 552  
activity in the foot region for a quasi-parallel shock, but the 553  
cause of the jump of the bulk plasma velocity is unclear; the 554  
same is true for its strong variation downstream. Both on 555  
DOY 042 and 045 the bulk plasma velocities downstream 556  
after the ramp make large excursions. The magnetic field 557  
values do not seem to support the hypothesis that the 558  
spacecraft crossed the shock front more than once during 559  
these intervals. The inbound shock crossing on DOY 055 is a 560  
quasi-parallel one; the outbound crossing is quasi-perpen- 561  
dicular. We have a gap in the SW data outbound, so it is 562  
difficult to comment on the slow bulk velocity decrease; it 563  
might be connected with the slow shock crossing as well. 564  
The DOY 057 crossing shows a bulk velocity jump quite 565  
typical for a perpendicular BS. However, the magnetic field 566  
variation is more complex: a substructure is evident between 567  
1300 and 1330 UT, and in the downstream region the heating 568  
is so weak that the proton and alpha distributions are still 569  
resolved in E/q. The strength of the shock potential (neglect- 570  
ing the pressure gradient contribution) can be assessed from 571  
 $1/2 m(u_{\text{up}}^2 - u_{\text{down}}^2)$ ; this yields  $\sim 100$  eV, half of the shock 572  
potential on DOY 012; there is no significant difference 573  
between the four crossings we are considering here. 574

[40] Despite the perturbed conditions the ion heating is 575  
sudden and sharp in all four cases, accompanied by a 576  
density jump and an electrostatic spike in the wave data. 577  
Thermalization can be used as a signature of the shock 578  
location even in those cases when the field data are rather 579  
smeared; it is a good indicator of shock location. 580

[41] The wave activity is high during all crossings, but in 581  
the ion data there is no direct evidence for reflected ions; 582  
that is, no single count was detected outside the SW 583  
direction. If the reflected particles had been propagating 584  
along the upstream magnetic field, they would have fallen 585  
into the FOV of IBS; specularly reflected ions could have 586  
been seen only on DOY 045. In Figure 13 we plot the 587  
thermal velocities of the SW ions for DOYs 042 and 045. In 588  
both cases the temperature values show strong modulations 589  
(possibly associated with the instabilities in the foot), but we 590  
could not yet identify correlation with the field data. We 591  
return to this issue in the next section. 592

[42] Though the quiet upstream and downstream regions 593  
are separated by hours, the real microstructure and the 594  
actual width of these shocks are a question. Taking into 595  
account the low incidence angles and the  $\sim 10$  km/s space- 596  
craft velocity, our preferred conclusion is that these shocks 597  
were exceptionally broad, but claims that only the crossing 598  
was slow cannot be excluded with certainty. 599

[43] The downstream ion distributions are generally per- 600  
turbed: single- and bi-Maxwellian distributions can both be 601  
seen as illustrated in Figure 14. A difficulty here is that IBS 602  
does not resolve mass, so we could not be sure about the 603  
true composition of the second peak or the tail. We are of 604

**Figure 12.** (opposite) A compilation of the plasma 915  
parameters for DOY 057, 1000–1700 UT. The notations 916  
are the same as in Figure 9. 917

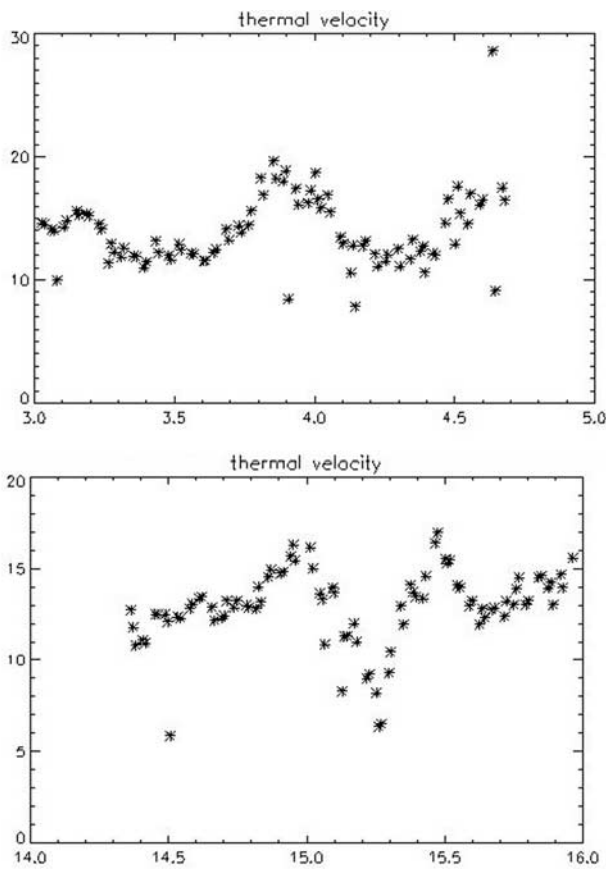


**Figure 13.** The solar wind thermal velocity for DOY 045 between 1420 and 1600 UT and for DOY 042 between 0300 and 0442 UT are shown. The horizontal axis exhibits time. The vertical axis is velocity in km/s.

605 the opinion, however, that this is the manifestation of the  
 606 perturbed post-ramp distributions seen in numerical simu-  
 607 lations [Leroy *et al.*, 1982] and many observations at the  
 608 Earth’s bow shock [e.g., Montgomery *et al.*, 1970].

609 [44] Strong magnetic turbulences are superimposed on  
 610 the magnetic fields. To exhibit these, we rotate the magnetic  
 611 field into a coordinate system in such a way that the  
 612 shock normal is parallel to the x-component. As shown in  
 613 Figure 15a, the magnetic field components are in phase  
 614 between 1325 UT and 1355 UT. Similar large-scale struc-  
 615 tures were seen in the magnetic field structures on DOY  
 616 042, as shown in Figure 15b. Andre *et al.* [2002] has  
 617 published an overview of the mirror mode fluctuations near  
 618 Jupiter during the Cassini flyby. The magnetic structures  
 619 seen on DOY 042, 1440–1450 UT, and on DOY 045,  
 620 1355–1400 UT, allow an interpretation that the fluctuations  
 621 are mirror modes. However, the low time resolution of  
 622 CAPS does not permit a correlation of the magnetic field  
 623 and particle data for these short time intervals. The magnetic  
 624 hodograms do not reveal any particular polarisation for the  
 625 whole interval shown in the figures.

626 **6. Discussion and Conclusions**

627 [45] In this paper we have presented the first results of the  
 628 measurements of the Jovian bow shock made by the

charged particle analyser CAPS carried on board the Cassini 629  
 spacecraft, together with supporting data from the magne- 630  
 tometer and the radio and plasma wave science instrument 631  
 RPWS. We have provided an overview of the SW properties 632  
 during the Jupiter flyby between 1 January and 30 March 633  
 2001, and we have discussed the structure of the transition 634  
 layer of the Jovian bow shock, focusing on five crossings. 635

[46] Cassini encountered Jupiter during a high solar 636  
 activity period. In the year 2000 and at the beginning of 637  
 2001 two magnetic sectors were present on the Sun up to 638  
 high latitudes, divided by one single warped current sheet 639  
 tilted slightly to the rotation axis of the Sun; the interplan- 640  
 etary magnetic field was significantly different from the low 641  
 solar activity situation. The observed magnetic field struc- 642  
 ture indicates that Cassini several times crossed current 643  
 sheet boundaries, and the SW velocity had a highly variable 644  
 structure, as seen from the ACE data (cf., Figure 2). Gurnett 645  
*et al.* [2002a, 2002b] detected three interplanetary shocks 646  
 (IPS) prior to the encounter between DOYs 320–360 in 647  
 2000; we reported an IPS on DOY 015, 2001, and other 648  
 IPSs were also crossed during this 90-day long interval. 649

[47] The Jovian bow shock must differ significantly from 650  
 that of the Earth. At the Earth the SW reaches the flank in a 651  
 few minutes, and the time needed for the magnetohydrody- 652  
 namical waves to travel between the obstacle and the bow 653  
 shock is minutes. At Jupiter it requires days till the SW 654  
 reaches the flank, and even at the nose the travel time can be 655  
 hours. In addition, as pointed out by Huddleston *et al.* 656  
 [1998], the obstacle itself is a quickly changing magneto- 657  
 disk. If we compare these time scales with the time scales of 658  
 solar wind fluctuations, it is conceivable that the Jovian bow 659  
 shock may seldom stay in a steady state, if it is reached at 660  
 all. A further complication arises from the high Mach 661  
 number because as Quest [1985] has pointed out, the normal 662  
 energy dissipation mechanisms that stabilize Earth’s bow 663  
 shock might not be adequate. Therefore the high variability 664  
 of the Jovian bow shock is not surprising. It is, however, a 665  
 nontrivial question how this variability should be mani- 666  
 fested. The drastically changing bow shock location, experi- 667  
 enced by all previous missions and by Cassini as well, is 668  
 such a signature, though it is also connected with the low 669  
 sheath density, in proportion with the low solar wind density 670  
 at Jupiter. Our intuition is driven here by a simple spring 671  
 model; a softer but longer spring makes larger excursions 672  
 but oscillates more slowly than a shorter and stronger one 673  
 (the spring length is connected with the bow shock obstacle 674  
 distance and the softness is connected with the sheath 675  
 density). We suggest other possible signatures of an un- 676  
 steady bow shock below, being aware that these have not 677  
 yet been explored in detail theoretically. 678

[48] The Cassini spacecraft crossed the Jovian bow shock 679  
 for the first time on 28 December 2000, at about 0419 UT. 680  
 Owing to favourable coincidence of the solar wind dynam- 681  
 ics and the spacecraft orbit, Cassini crossed the shock front 682  
 about 40 more times in the ecliptic plane on the duskside. 683  
 This side was not explored by the first four space missions 684  
 targeting Jupiter, and because of the fast corotation of the 685  
 Jovian magnetosphere, no trivial symmetry can be expected 686  
 between the dawn and dusk sides. In this sense, even the 687  
 phenomenological description of the bow shock crossings 688  
 provides new, important insight. In this paper we have 689  
 presented the detailed description of five BS crossings, 690

691 one around 1930 LT, other four between 2100 and 2200 LT.  
 692 The Jovian bow shock is huge, extending over 700 R<sub>J</sub> from  
 693 the planet, and Cassini was the first spacecraft experiencing  
 694 such distant bow shock crossings.  
 695 [49] An important conclusion is that even in those cases  
 696 when the magnetic field and wave structures would not  
 697 allow an easy determination of the shock location, the onset  
 698 of proton thermalization is a good signature of it. The

thermalization sets in at a very short characteristic time 699  
 scale, accompanied by a jump in bulk plasma density. At 700  
 the same location we have always observed a relatively 701  
 strong electrostatic pulse in the proton plasma frequency 702  
 range, possibly due to electrostatic ion waves [Wu et al., 703  
 1984]. Thomsen et al. [1985] has found such fast proton 704  
 thermalization at the ramp of the Earth bow shock for Mach 705  
 numbers close to the critical value. They have argued that the 706  
 bulk ion heating might be caused by modified two-stream 707  
 instability driven by cross-field currents within the shock, 708  
 and ion acoustic instability, driven by field-aligned beam. In 709  
 those studies, however, the magnetic field was always a 710  
 good indicator of the shock surface; therefore the question of 711  
 whether thermalization is a good shock indicator even if the 712  
 magnetic field is not was not raised. In our case all the 713  
 shocks are supercritical, or the Mach numbers are even 714  
 higher than the second critical Mach number. The picture 715  
 we suggest is the following: in addition to the wave 716  
 excitation modes described above, it is known that density 717  
 gradient at the shock ramp can be the source of free energy 718  
 for lower hybrid drift instabilities [cf., Wu et al., 1984, 719  
 equation (8)], and such lower hybrid waves can effectively 720  
 heat ions. Though the details should be worked out, we 721  
 suggest that the location of the density gradient manifests 722  
 itself in lower hybrid wave excitation that subsequently heats 723  
 ion. This is the reason why thermalization can be used to find 724  
 the location of the ramp for high Mach number shocks. 725

[50] The next finding is that at the flanks, between 2100 726  
 and 2200 LT, the shock transition layer (defined as the 727  
 region extending from quiet upstream to quiet downstream) 728  
 is very much perturbed and broad. The energy loss of the 729  
 bulk upstream particle population is about half of what was 730  
 observed at 1930 LT. The weakening of the shock potential 731  
 towards the flank in certain models is frequently associated 732  
 with the decrease of the local Mach number derived from 733  
 the component of the solar wind perpendicular to the shock 734  
 front. Lee and Wu [2000, Figure 9] showed using hybrid 735  
 simulations that the correlation between shock potential 736  
 jump and shock Mach number is not linear; in their model 737  
 the shock potential drops both for very high and very low 738  
 Mach numbers. In our cases the Mach number was higher 739  
 than at earlier local times, and the shock potential was much 740  
 weaker. 741

[51] When we cross the bow shock the variation of the 742  
 plasma parameters from the upstream regions to downstream 743  
 more frequently defies expectations than otherwise. Where- 744  
 as the Rankine-Hugoniot relations correctly described the 745  
 bulk plasma properties in cases when the magnetic field 746  
 indicated a clear discontinuity as well, in other cases the 747  
 bulk plasma velocity exceeds upstream velocity values within 748  
 the shock transition layer and makes large excursions. We do 749

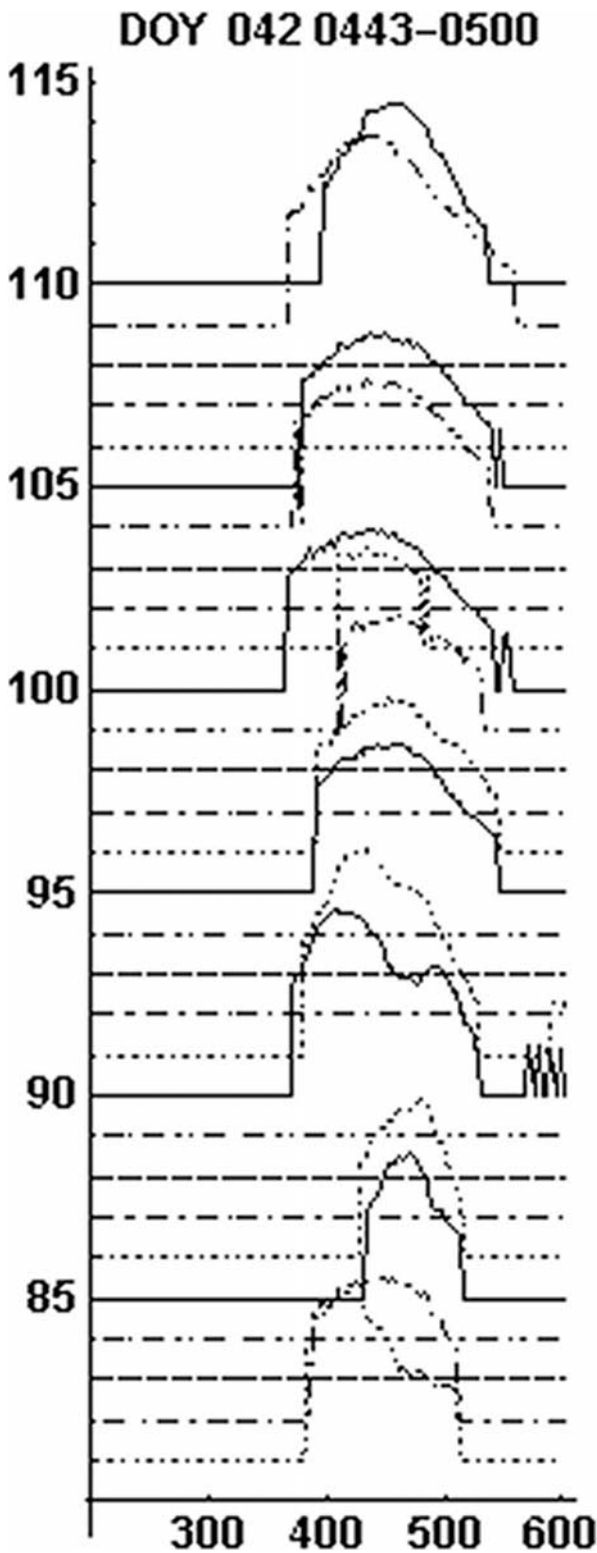


**Figure 14.** (opposite) IBS velocity log counts spectra are shown. The horizontal axis is velocity in km/s units. The spectra, measured in each 32 s are shown in vertical arrangement; time flows upward. As the plasma flow is not always in the field of view of the actuator, there are “zero-count” spectra as well. The middle position of the actuator for these spectra, starting from below, are 93, 89, 64, 58, 80, 96, 80, 58, 63, 88, 92, 69, 56, 72, 94, 87, 62, 58, 80, 58, 80, 57, 62, 87, 93, 72, 57, 72, and 93 degrees.

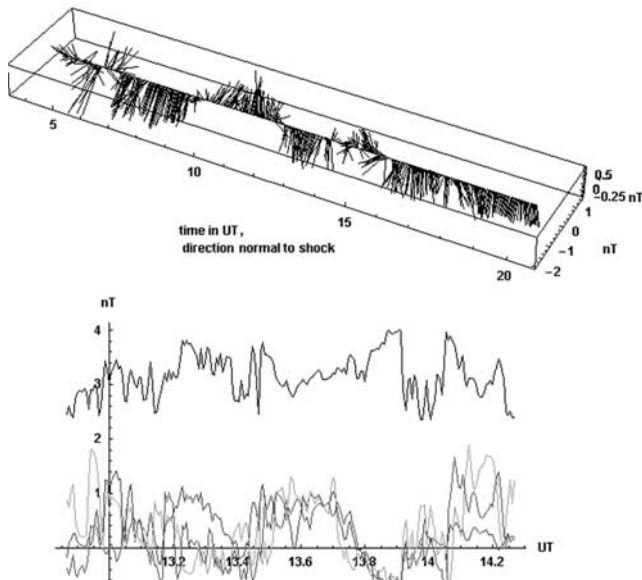


**Figure 15.** (a) The magnetic field perturbations downstream of the shock of DOY 045, when the x-component is along the shock normal. The horizontal axis is time in UT, and the vertical axis is magnetic field in nT. Shown are the x (red), z (blue), and  $-y$  (green) components of the magnetic field, the latter decreased by 1 nT. The black line is the total field, shifted by 2 nT upwards. (b) Long wavelength standing waves downstream of the shock on DOY 042. The horizontal axis is time in UT measured along the direction of the shock normal; the other axes are magnetic field components in nT.

not have any explanation of that or of the behavior of other fields and plasma parameters. These can certainly be associated with variations in the solar wind, but we believe that more complex explanation is needed. The bow shock seems to be very broad at the flank; further work is needed to find out the substructures seen in the transition layer.

[52] The high variability of the Jovian bow shock was confirmed by all previous missions. We are of the opinion that many of the observed features are indicative of the nonequilibrium state of the BS. In equilibrium, for quasi-perpendicular shocks, there is time for the wave steepening and for all the well-known shock structures to develop; probably the opposite is true for nonequilibrium. Therefore it is conceivable that the large variety of magnetic wave-like structures superimposed on the shock front might be connected with the lack of equilibrium. We have illustrated their presence in the paper. For the time being this is a conjecture only; we are not really aware of techniques that can treat such problems.

[53] Reflected protons were not detected upstream the bow shock above our current sensitivity limit. *Gosling and Robson* [1985] argued that particles are specularly reflected if their energy is lower than the shock potential. These are either returned to the shock front by the ambient magnetic field or they are streaming back upstream. A different population may propagate along the magnetic field lines [Thomsen, 1985]. Both directions were in our FOV on DOY 012, and the magnetic field direction was in the FOV for all cases. Therefore it is somewhat surprising that we did not

detect them because about a quarter of the protons should have been reflected. Our explanation is that the reflected protons are expanding quickly in the phase space, and even though CAPS looked into the right directions, the particle densities were below the sensitivity threshold. Wave data collected in the foot region of the bow shock indicate the presence of a reflected particle distribution. In the foot region the SW becomes perturbed, and its temperature is modulated. In the simulation of *Quest* [1985], fluctuations in reflected particle distributions indicate shock instability when the Mach number is high. The observed SW temperature fluctuations (with  $M_A \sim 18$  in one case) might be connected with this fact. We do not discuss further foot phenomena here, but this will be the topic of separate publications.

[54] In summary, in this paper we have presented the phenomenology of the Jovian bow shock as observed by the CAPS instrument onboard the Cassini spacecraft. Cassini explored the duskside of the bow shock in the ecliptic plane, which was not visited by previous missions. No previous mission observed such an extended shock, still present more than  $700 R_J$  away from Jupiter. The shock transition layer at the flank was broad and very much perturbed, but the onset of the ion thermalization, accompanied by a fairly strong electrostatic wave pulse and a jump in bulk plasma density, was always fast. The bulk plasma behaviour in the broad transition layer is not understood yet. In the foot region the reflected ions were below CAPS sensitivity limit; their presence however is suggested by the field data and by the observed changes in the solar wind. We have conjectured that most of the observations indicate an unsteady bow shock, but the physical interpretation of the observation will be the focus of future works.

[55] **Acknowledgments.** The work of K. S. was supported by the Hungarian OTKA grant T-32634. The research at The University of Iowa was supported by NASA through contract 961152 through the Jet Propulsion Laboratory. Work at MSSL-UCL was supported by PPARC.

[56] Lou-Chuang Lee thanks B. H. Wu and another reviewer for their assistance in evaluating this paper.

**References**

Andre, N., G. Erdos, and M. K. Dougherty, Overview of mirror mode fluctuations in the jovian dusk magnetosheath: Cassini magnetometer observations, *Geophys. Res. Lett.*, 29(20), 1980, doi:10.1029/2002GL015187, 2002. 818

Balogh, A., M. K. Dougherty, R. J. Forsyth, D. J. Southwood, E. J. Smith, B. T. Tsurutani, N. Murphy, and M. E. Burton, Magnetic field observations during the Ulysses flyby of Jupiter, *Science*, 257, 1515–1518, 1992. 821

Bame, S. J., et al., Jupiter’s magnetosphere: Plasma description from the Ulysses flyby, *Science*, 257, 1539–1543, 1992. 822

Cravens, T. E., *Physics of Solar System Plasmas*, Cambridge Univ. Press, New York, 1997. 823

Dougherty, M. K., et al., The Cassini magnetic field investigation, *Space Sci. Rev.*, in press, 2002. 824

Gosling, J. T., and A. E. Robson, Ion reflection, gyration, and dissipation at supercritical shocks, in *Collisionless Shocks in the Heliosphere: Review of Current Research*, *Geophys. Monogr. Ser.*, vol. 35, edited by B. T. Tsurutani and R. G. Stone, pp. 141–152, AGU, Washington, D. C., 1985. 825

Gurnett, D. A., et al., Control of Jupiter’s radio emission and aurorae by the solar wind, *Nature*, 415, 985, 2002a. 826

Gurnett, D. A., et al., The Cassini radio and plasma wave investigation, *Space Sci. Rev.*, in press, 2002b. 827

Hill, W. H., Magnetic moments at Jupiter, *Nature*, 415, 965, 2002. 828

Huddleston, D. E., C. T. Russell, M. G. Kivelson, K. K. Khurana, and L. Bennett, Location and shape of the Jovian magnetopause and bow-shock, *J. Geophys. Res.*, 103, 20,075–20,082, 1998. 829

Kivelson, M. G., et al., Galileo at Jupiter: Changing states of the magnetosphere and first looks at Io and Ganymede, *Adv. Space Res.*, 20, 193–204, 1997. 830

- 846 Kurth, W. S., et al., An overview of observations by the Cassini radio and  
847 plasma wave investigation at Earth, *J. Geophys. Res.*, 106, 30,239, 2001.
- 848 Lee, L. C., and B. H. Wu, Heating and acceleration of protons and minor ions  
849 by fast shocks in the solar corona, *Astrophys. J.*, 535, 1014–1026, 2000.
- 850 Leroy, M. M., et al., The structure of perpendicular bow shock, *J. Geophys.*  
851 *Res.*, 87, 5081, 1982.
- 852 Lever, E. L., et al., Shock surfing versus shock drift acceleration, *Geophys.*  
853 *Res. Lett.*, 28, 1367, 2001.
- 854 Linder, D. R., et al., The Cassini CAPS electron spectrometer, in *Measure-*  
855 *ment Techniques in Space Plasmas: Particles*, *Geophys. Monogr. Ser.*,  
856 vol. 102, edited by R. Pfaff, J. Borovsky, and D. Young, pp. 257–262,  
857 AGU, Washington, D. C., 1998.
- 858 Montgomery, M. D., J. R. Asbridge, and S. J. Bame, Vela 4 plasma ob-  
859 servations near the earth's bow shock, *J. Geophys. Res.*, 75, 1217, 1970.
- 860 Moses, S. L., F. V. Coroniti, C. F. Kennel, and F. L. Scarf, Estimation and  
861 comparison of quasilinear electron heating in the shock foot at Jupiter and  
862 Earth, *Geophys. Res. Lett.*, 12, 609–612, 1985.
- 863 Moses, S. L., F. V. Coroniti, C. F. Kennel, W. S. Kurth, and D. A.  
864 Gurnett, Comparison of plasma wave measurements in the bow shocks  
865 at Earth, Jupiter, Saturn, Uranus and Neptune, *Geophys. Res. Lett.*, 17,  
866 1653, 1990.
- 867 Quest, K. B., Simulation of high Mach number collisionless perpendicular  
868 shocks in astrophysical plasmas, *Phys. Rev. Lett.*, 54, 1872–1874, 1985.
- 869 Scarf, F. L., D. A. Gurnett, and W. S. Kurth, Measurements of plasma wave  
870 spectra in Jupiter's magnetosphere, *J. Geophys. Res.*, 86, 8181–8198,  
871 1981.
- 872 Scarf, F. L., S. L. Moses, C. F. Kennel, E. W. Greenstadt, and F. V. Coroniti,  
873 Plasma waves near collisionless shocks, in *Proceedings of the Interna-*  
874 *tional Conference on Collisionless Shocks in Balatonfured, Hungary*,  
875 edited by K. Szego, pp. 19–41, Cent. Res. Inst. for Phys., Budapest,  
876 Hungary, 1987.
- 877 Scudder, J. D., E. C. Sittler, and H. S. Bridge, A survey of the plasma  
878 electron environment of Jupiter: A view from Voyager, *J. Geophys. Res.*,  
879 86, 8157–8179, 1981.
- 880 Smith, E. J., et al., Ulysses in the south polar cap at solar maximum:  
881 Heliospheric magnetic field, *Geophys. Res. Lett.*, 28, 4159, 2001.
- 882 Stone, R. G., et al., Ulysses radio and plasma wave observations in the  
883 Jupiter environment, *Science*, 257, 1524–1531, 1992.
- 884 Thomsen, M. F., Upstream suprathermal ions, in *Collisionless Shocks in the*  
885 *Heliosphere: Review of Current Research*, *Geophys. Monogr. Ser.*, vol.  
886 35, edited by B. T. Tsurutani and R. G. Stone, pp. 253–270, AGU,  
887 Washington, D. C., 1985.
- Thomsen, M. F., J. T. Gosling, S. J. Bame, and M. M. Mellott, Ion and 888  
electron heating near the critical Mach number, *J. Geophys. Res.*, 90, 889  
137–148, 1985.
- Wu, C. S., et al., Microinstabilities associated with a high Mach number, 891  
perpendicular bow shock, *Space Sci. Rev.*, 37, 63, 1984.
- Young, D. T., et al., Cassini plasma spectrometer investigation, in *Measure-* 893  
*ment Techniques in Space Plasmas*, *Geophys. Monogr. Ser.*, vol. 102, 894  
edited by R. E. Pfaff, J. E. Borovsky, and D. T. Young, pp. 237, AGU, 895  
Washington, D. C., 1998.
- Young, D. T., et al., Cassini plasma spectrometer investigation, *Space Sci.* 897  
*Rev.*, in press, 2002.
- Vilppola, J. H., P. J. Taskanen, B. L. Barraclough, and D. J. McComas, 899  
Comparison between simulations and calibrations of a high resolution 900  
electrostatic analyzer, *Rev. Sci. Instr.*, 72, 3662–3669, 2001. 901
- 
- B. Barraclough and M. F. Thomsen, Los Alamos National Laboratory, 902  
Space and Atmospheric Science Group, Los Alamos, NM 87545, USA. 904  
(bbarraclough@lanl.gov; mthomsen@lanl.gov) 905
- J.-J. Berthelier, Centre d'Étude des Environnements Terrestre et 906  
Planétaires, Observatoire de Saint-Maur, 4 Avenue de Neptune, 94107 St. 907  
Maur-des-Fosses Cedex, France. (jean-jacques.berthelier@cetp.ipsl.fr) 908
- F. J. Crary, University of Michigan, 2455 Hayward Street, Ann Arbor, MI 909  
48109, USA. (fcrary@umich.edu) 910
- D. J. McComas and D. T. Young, Division of Space Sciences and 911  
Engineering, Southwest Research Institute, 6220 Culebra Road, P. O. 912  
Drawer 28510, San Antonio, TX 78228-0510, USA. (dmccomas@swri. 913  
edu; dyoung@swri.edu) 914
- A. J. Coates, University College London, Mullard Space Science 915  
Laboratory, Holmbury St. Mary, Dorking, Surrey RH5 6NT, UK. (ajc@ 916  
mssl.ucl.ac.uk) 917
- M. K. Dougherty, Blackett Laboratory, Imperial College, Prince Consort 918  
Road London, SW7 2 BW, UK. (m.dougherty@ic.ac.uk) 919
- G. Erdos and K. Szego, KFKI Research Institute for Particle and Nuclear 920  
Physics, Konkoly Thege str. 29-33, Bldg. III, H-1121 Budapest, Hungary. 921  
(erdos@rmki.kfki.hu; szego@rmki.kfki.hu) 922
- D. A. Gurnett and W. S. Kurth, Department of Physics and Astronomy, 923  
The University of Iowa, 203 Van Allen Hall, Iowa City, IA 52242-1479, 924  
USA. (donald-gurnett@uiowa.edu; william-kurth@uiowa.edu) 925